ANALYSIS OF LOCAL TRANSPORT IN NEUTRAL-BEAM-HEATED L AND H PLASMAS OF ASDEX

G. Becker, ASDEX Team[+] and Neutral Injection Team[++]

IPP III/98

June 1984

MAX-PLANCK-INSTITUT FÜR PLASMAPHYSIK

8046 GARCHING BEI MÜNCHEN

MAX-PLANCK-INSTITUT FÜR PLASMAPHYSIK

GARCHING BEI MÜNCHEN

ANALYSIS OF LOCAL TRANSPORT IN NEUTRAL-BEAM-HEATED L AND H PLASMAS OF ASDEX

G. Becker, ASDEX Team[+] and Neutral Injection Team[++]

IPP III/98 June 1984

Die nachstehende Arbeit wurde im Rahmen des Vertrages zwischen dem Max-Planck-Institut für Plasmaphysik und der Europäischen Atomgemeinschaft über die Zusammenarbeit auf dem Gebiete der Plasmaphysik durchgeführt.

IPP III/98

G. Becker, ASDEX Team[+]
and Neutral Injection Team[++]

ANALYSIS OF LOCAL TRANSPORT IN NEUTRAL-BEAM-HEATED L AND H PLASMAS OF ASDEX

June 1984

ABSTRACT. A well-diagnosed series of high-confinement (H) discharges in ASDEX is studied in detail by transport modelling. Computed temperature and density profiles in the Ohmic and H phases are compared with measurements. Profiles for the electron heat diffusivity χ_e, diffusion coefficient D and inward drift velocity v_{in} are determined for the whole plasma including the scrape-off zone. Empirical scaling relations of these quantities in the L and H regimes are presented. The development of density and temperature profiles after transition to the H phase is investigated. The inward drift with neutral injection is studied.

1. Introduction

The operation of tokamaks like ASDEX has demonstrated that in the axisymmetric divertor configuration clean plasmas can be produced with Ohmic and neutral injection heating. It is well known that discharges with very low impurity levels are suitable for confinement studies, since impurity radiation does not mask transport processes such as heat conduction. Apart from that these plasmas are attractive for the investigation of transport, because the observed L (low) and H (high confinement) modes of operation /1,2/ yield a larger range of parameter variation.

Flux-surface averaged transport in L and H discharges of ASDEX has been analyzed before by computer simulation /3-5/. The present paper deals with the detailed analysis of a well-diagnosed series of H discharges

---

[+]K. Bernhardi, A. Eberhagen, G. Fussmann, O. Gehre, J. Gernhardt, G.v.Gierke, E. Glock, G. Haas, F. Karger, M. Keilhacker, S. Kissel, O. Klüber, M. Kornherr, K. Lackner, G. Lisitano, H.M. Mayer, K. McCormick, D. Meisel, E.R. Müller, H. Murmann, H. Niedermeyer, W. Poschenrieder, H. Rapp, H. Röhr, F. Schneider, G. Siller, P. Smeulders, F. Söldner, K.-H. Steuer, F. Wagner

[++]G.G. Lister, E. Speth, A. Stäbler, O. Vollmer

in double-null divertor configuration with plasma current I_p = 380 kA and injection power P_{NI} = 3.2 MW.

A short summary of the modelling with the BALDUR transport code is given in Section 2. In Section 3, results of measurements and simulations are compared. The corresponding profiles of χ_e, D and v_{in} in the whole plasma including the scrape-off region are presented and discussed. The time development of n and T_e profiles after transition to the H phase is studied. A relation yielding a self-consistent description of the anomalous inward flux is applied. Finally, in Section 4 expressions for the inward drift velocity are derived from the particle balance equation with neutral injection and compared with results from modelling.

2. Modelling

The transport simulations are carried out with modified versions (BALDIO9R) of the BALDUR prediction transport code /6/ which are described in Refs. /3,7,8/. Nevertheless, we summarize here some of the essential ingredients of the model.

The transport code is one-dimensional and has essentially three radial zones. In the innermost region $r < r_{q=1}$ the effect of sawteeth on transport is taken into account by adding $D_B f_q$ terms to the diffusivities, where D_B is the Bohm diffusion coefficient and f_q is a q-dependent function. The second zone $r_{q=1} < r < 0.9\ r_s$ with separatrix radius r_s = 40 cm is called "confinement zone". The outermost zone $r_s < r < r_w$ with wall radius r_w = 49 cm is the scrape-off region. In the range $0.9\ r_s < r < r_s$ the coefficients of the confinement and scrape-off zones are connected by a linear transition. A non-equidistant grid with 20 out of 50 grid points in the scrape-off region is used.

The code has been made more suitable for modelling divertor tokamaks with collision-dominated scrape-off plasmas by implementing a scrape-off-region model which separately treats heat conduction and convection losses to the divertor /3,7,8/. The heat flux density is described by classical electron thermal conductivity $\|\vec{B}$ yielding $q_{e\|}(r) \sim T_e(r)^{7/2}$.

A flow velocity equal to 1/7 of the ion sound velocity is used to model the convective particle and energy losses.

In order to produce more realistic density profiles Ware pinch terms have been replaced by an anomalous inward flux of the form nv_{in} in the continuity and energy equations. This avoids shoulders or even side-maxima on the density profiles and scrape-off densities much higher than observed, which would lead to strong absorption of injection power in the scrape-off plasma.

3. Results from transport analysis

In this Section results from modelling a series of H discharges and scaling relations for transport coefficients which have been derived from many series of L and H discharges in ASDEX are presented first. Then, special attention is paid to the development of n and T_e profiles after the L to H transition and to the role of the anomalous inward flux.

3.1 Determination of χ_e, D and v_{in} profiles

A well-diagnosed series of double-null divertor H discharges with plasma current I_p = 380 kA and neutral injection power P_{NI} = 3.2 MW is analyzed in detail. In this series hydrogen beams are injected tangentially in the co-direction into deuterium target plasmas. The measured time developments of I_p and the line-averaged density $\bar{n}_e$, shown in Fig. 1, are prescribed in the computations. The beginning of the H phase is marked by t^*. In Fig. 2 profiles of density and electron temperature measured at 1.0 s are compared with simulations (solid curves). Agreement is also obtained with the measured $\beta_p \simeq 0.3$, energy confinement time $\tau_E \simeq 70$ ms and neutron production rates. In the confinement zone the OH scaling is applied, i.e. $\chi_e = 2.5 \times 10^{17}\ n_e^{-1}\ T_{e,keV}^{-1}\ q^{-1} cm^2 s^{-1}$ and $D = 0.2\ \chi_e$. The corresponding profiles of χ_e, D and $v_{in} = 150\ r/r_w$ cm s^{-1} are shown in Fig. 3. The ion heat diffusivity χ_i used is 1 time the neoclassical value according to Ref. /9/.

Applying the diffusivities $\chi_e = 1.2 \times 10^4$ cm^2 s^{-1} and $D = 1.4 \times 10^3$ cm^2 s^{-1} in the scrape-off region yields the measured exponential decay

lengths $\lambda_{Te} \simeq 1.0$ cm and $\lambda_n \simeq 1.5$ cm. Typically, about 80 % of the absorbed power is transported to the divertor, the dominant loss channel being electron thermal conduction. Results from a detailed study of the physical processes in the scrape-off layer of poloidal divertor tokamaks are given in Ref. /10/.

After the beams are switched on, the confinement of the Ohmic phase persists for a time span $(\Delta t)_{on} \simeq 40$ ms /3,4/. Then, a different transport with enhanced diffusivities which do not depend on density but on B_p appears and replaces the OH scaling. Reaching this phase of enhanced transport seems to be necessary for the development of the H confinement, since the H phase always starts later. This suggests that the transport mechanism of the H regime is closely related to the processes responsible for the L confinement /4/. In the series under investigation the abrupt transition to the H type occurs at t^* after a rather short L phase with enhanced losses. The H phase can be modelled by changing the diffusivities χ_e and D and the inward drift velocity at t^*.

Profiles of density and electron temperature measured at 1.25 s are compared with computed results (solid curves) in Fig. 4. Again agreement is also obtained with measured $\beta_p \simeq 1.5$ and $\tau_E \approx 50$ ms. The corresponding profiles for χ_e, D and v_{in} are shown in Fig. 5. They result from the following empirical scaling relation which can be expressed by dimensionless quantities

$$\chi_e^H = 9.2 \times 10^3 \, r_n^{-1/2} \, T_i^{1/2}[\text{keV}] \, r \, B_p^{-1}[\text{kG}] \ \text{cm}^2 \ \text{s}^{-1} \qquad (1)$$

with $r_n^{-1} = -\frac{1}{n}\frac{\partial n}{\partial r}$ and $D^H = 0.2 \, \chi_e^H$ and from $v_{in} = 300 \, (r/r_w)^2$ cm s^{-1} which produces the observed broader density profiles of the H phase. The $\chi_e(r)$ is consistent with the flat χ_e profiles obtained in earlier simulations of H discharges by using test functions /4/. It is found that applying the right profiles for the diffusivities is of primary importance. In a predictive code analysis it is convenient to utilize scaling relations of transport coefficients. The empirical scaling relation of Eq. (1) yields a good fit to all series of H discharges in ASDEX analyzed so far.

Usually, there are observed in H discharges burst-like energy and particle losses from a zone $r_s/2 \lesssim r \lesssim r_s$ which result from edge localized mode activity. In the above simulations the time-average over these additional fluxes has been modelled by electron heat conduction and diffusion. Consequently, the diffusivities for the undisturbed H phases are still lower than those given in Eq. (1).

The scaling of Eq. (1), but with a 2.5 times larger numerical factor, is capable of modelling all series of L discharges with flat χ_e profiles (LI type) /4/ analyzed up to now:

$$\chi_e^L = 2.3 \times 10^4 \; r_n^{-1/2} \; T_i^{1/2}[\mathrm{keV}] \; r \; B_p^{-1}[\mathrm{kG}] \; \mathrm{cm}^2 \; \mathrm{s}^{-1} \qquad (2)$$

and $D^L = 0.2 \; \chi_e^L$. As an example the simulation of an L discharge with I_p = 320 kA and P_{NI} = 1.4 MW is given. In Fig. 6 computed n_e and T_e profiles (solid curves) at the end of the injection period are compared with measurements. The χ_e^L scaling also yields τ_E = 30 ms and β_p = 0.6 in agreement with measured data. At present, the accuracy of experimental data and the range of parameter variation are not sufficient to exclude modified representations of $\chi_e(r)$, e.g. by other profile scale lengths.

As in the Ohmic phase χ_i is about 1 time the neoclassical value /9/. It is found that the diffusivities χ_e and D in the scrape-off zone do not have to be changed compared with the Ohmic phase in order to yield the measured $\lambda_{Te} \lesssim 1.0$ cm and $\lambda_n \simeq 1.5$ cm. Moreover, the electron temperature gradient near the separatrix at $r \lesssim r_s$ also agrees with the measurements. With $\chi_e < 1.2 \times 10^4$ cm^2 s^{-1} in the scrape-off region one obtains λ_{Te} smaller and T_e gradients larger than those observed. In the opposite case λ_{Te} becomes too large and the "pedestal" on the T_e profile disappears. Reducing χ_e in the scrape-off plasma to the correct value $\chi_e = 1.2 \times 10^4$ cm^2 s^{-1} shows that a pedestal is not produced for the whole T_e profile, because the central temperatures are not increased as much as those near the edge. Consequently, the thermal energy content and τ_E rise by only 10 %, while a pedestal of about 300 eV for the whole T_e profile should improve τ_E by roughly 25 % with a volume-averaged electron temperature of 1.2 keV.

The hypothesis of a thermally insulating sheath at the plasma edge which only develops in H discharges and leads to the improved confinement is not supported by the measured electron temperature profiles. The corresponding χ_e profiles in L and H discharges show almost the same decrease in the edge region.

After a higher thermal energy content is built up in the H phase owing to better confinement, the energy flux over the separatrix reaches the value in L discharges, i.e. typically 80 % of the total input. As this power is

transported to the divertors mainly by parallel electron heat conduction ($q_{\parallel}(r) \sim T_e(r)^{7/2}$) /3,7,8/, the same energy loss in L and H discharges is consistent with the same values for $T_e(r_s)$ and λ_{Te} which are indeed measured in L and H plasmas of ASDEX. It is concluded that the electron heat conduction $\parallel \vec{B}$ in the scrape-off plasma is not inhibited during the H phase /11/.

3.2 Time behaviour of n and T_e profiles after transition to the H phase

Earlier computer analysis of the measured time development of electron temperature profiles in the H phase /4/ has shown that a sudden reduction of χ_e takes place throughout the plasma at t^*. The observed time behaviour of the line-averaged density in H discharges with constant gas-puff rate can also be modelled by an abrupt reduction of D by a factor of two at t^* /4/. Both results are consistent if D continues to be coupled to χ_e, as the simulations have shown.

In H discharges which are not triggered by a sawtooth a smooth variation of $T_e(r,t)$ after t^* is observed. Local transport analysis shows that this change in electron temperature profile results from reducing χ_e at t^* and from broadening the density and beam-heating profiles. This means that there is no sudden change in electron temperature profile that triggers the L to H transition.

3.3 Self-consistent computation of anomalous inward fluxes

In addition to the diffusivities χ_e and D the inward drift velocity has to be changed in the H phase as shown in Section 3.1. Whether v_{in} influences the L-to-H-transition or not is studied by trying to compute it self-consistently instead of prescribing its profiles in the various phases.

By applying the following relation for the inward drift velocity based on a thermoelectric-type effect

$$v_{in} = -0.54\, D\left(\frac{r_s}{2}\right) T_e^{-1} \frac{\partial T_e}{\partial r} \text{ cm s}^{-1} \qquad (3)$$

one succeeds in producing the density profiles of Section 3.1 in all phases of the discharge and the necessary v_{in} profiles self-consistently as shown in Fig. 7. Obviously, the steeper v_{in} profile during the H phase is automatically obtained. According to the above scaling this change in $v_{in}(r)$ results from the smooth variation of the electron temperature profile and consequently does not trigger the transition to the H phase.

Self-consistent v_{in} profiles from Eq. (3) yield a modelling of the present series of H discharges which is as good as the simulations with prescribed v_{in} profiles. The differences are smaller than the experimental error. The v_{in} scaling has been applied in other series of H discharges with longer L phases and was found to be applicable.

4. Anomalous inward flux with neutral injection

The objective of this Section is to derive relations for the inward drift velocity from particle balance in the case of neutral-beam heating which can be checked against results from simulations.

Under steady-state conditions the particle balance equation with anomalous outward diffusion and anomalous inward convection reads

$$-D \frac{\partial n}{\partial r} - n\, v_{in} = \Gamma_D + \Gamma_b \qquad (4)$$

where Γ_D and Γ_b are the flux densities due to ionization of cold D atoms and due to neutral injection, respectively.

In plasmas which are impermeable to cold neutrals ($\lambda_o \ll a$ with mean free path λ_o and plasma radius a) Γ_D is located near the edge and is very weak in the bulk plasma. In Ohmically heated discharges Γ_D is typically one order of magnitude smaller than the diffusive and convective flux densities.

With neutral injection heating the situation is quite different. Except for the edge region the dominant particle source is Γ_b, which is of the order of the diffusive and convective terms. Neglecting Γ_D in Eq.(4) yields

$$v_{in} \simeq D\, r_n^{-1} - \frac{\Gamma_b}{n} \qquad (5)$$

with the inverse scale length $r_n^{-1} = -\frac{1}{n}\frac{\partial n}{\partial r}$.

The expression $v_{in} \simeq D r_n^{-1} \approx \frac{2}{a^2} Dr$ for Ohmically heated plasmas ($\Gamma_b = 0$) and parabolic density profiles is no longer valid in the L and H phases, since the term due to neutral injection cannot be neglected. This becomes obvious from L discharges, where D and r_n^{-1} are markedly increased. The inward drift velocity would be considerably enhanced, which contradicts the results from modelling.

More generally, an inward drift velocity which linearly depends on D is incompatible with the particle balance in the case of neutral injection. Inserting $v_{in} = Df(r)$ into Eq. (4) with $\Gamma_D = 0$ and dividing by D shows that n(r) still depends on the diffusion coefficient and becomes broader with increasing D. According to Eq. (5) this means that the inward drift velocity exhibits a D dependence which is weaker than linear. This conclusion is consistent with the v_{in} relation of Eq. (3), since $T_e^{-1}\partial Te/\partial r$ is an implicit function of χ_e or D.

If charge exchange, radiation and convective energy losses are negligible compared with the electron heat conduction, one can write approximately for $P_b \gg P_{OH}$

$$-n\chi_e \frac{\partial Te}{\partial r} \simeq P_b(r) = \Gamma_b(r)\, \bar{E}(r)$$

where $\bar{E}$ is the average energy per injected particle and a weak function of radius.

Replacing Γ_b in Eq. (5) and setting $\chi_e = 5D$ yields

$$v_{in} \simeq D(r_n^{-1} - 5\frac{T_e}{\bar{E}}\, r_{Te}^{-1}) \qquad (6)$$

with the inverse scale length $r_{Te}^{-1} = -\frac{1}{Te}\frac{\partial Te}{\partial r}$. The neutral injection enters by the average energy per injected particle, by shaping the density profile and by determining the electron temperature gradient.

5. Conclusions

For a series of H discharges local transport in the whole plasma including the scrape-off region was analyzed by computer simulations. Profiles of coefficients χ_e, D and ν_{in} were determined in the Ohmic and H phases by comparing measured and computed electron temperature and density profiles.

Measured electron temperature profiles in the scrape-off zone can be modelled by homogeneous $\chi_e = 1.2 \times 10^4$ cm^2 s^{-1} in the Ohmic and H phases. This value is found to be also consistent with the measured pedestal in the T_e profile within the separatrix, whereas larger or smaller χ_e values are not. Varying this quantity revealed that the global energy confinement time is improved by only 10 % owing to the pedestal. Thus, it cannot explain τ_E being a factor of roughly two larger in H discharges than in the L type. The improved confinement is due rather to a reduction of the diffusivities χ_e and D throughout the plasma. As there are no marked differences in the shape of χ_e profiles in L and H discharges of ASDEX, one can exclude the hypothesis of the better H confinement being due to a thermally insulating sheath that only exists in the H phase.

Electron temperature profiles measured in the outer plasma and in the scrape-off zone also contradict the idea that parallel electron heat conduction to the divertors is inhibited in the H phase.

The empirical scaling relation $\chi_e^L = 2.3 \times 10^4\ r_n^{-1/2}\ T_i^{1/2}[\mathrm{keV}]\ r\ B_p^{-1}[\mathrm{kG}]$ cm^2 s^{-1} and $D^L = 0.2\ \chi_e^L$ was determined from all series of LI discharges in ASDEX analyzed so far. The same scaling, but with a 2.5 times smaller numerical factor, is capable of modelling all H series studied before and the present H series under investigation. As in earlier simulations flat profiles are obtained for the diffusivities. According to this scaling local transport coefficients are independent of density like τ_E. They depend on the lcoal quantities B_p and T_i, which correspond to the global parameters I_p and P_{NI} in the τ_E scaling. Modified parameter representations cannot be excluded, this being particularly true in the case of possible dependences on profile scale lengths.

In agreement with the earlier studies of transport in the OH, L and H phases neoclassical values of the ion heat diffusivity were found.

The computations have further shown that the observed variation of the T_e profile does not trigger the L to H transition but rather represents the response to the drop of χ_e and to the broadening of density and injection-heating profiles.

With the scaling $v_{in} = -0.54\ D(\frac{r_s}{2})\ T_e^{-1}\ \frac{\partial T_e}{\partial r}$ cm s^{-1} a self-consistent modelling of the v_{in} profiles in the OH, L and H phases was achieved. This suggests that the L to H transition is not triggered by a sudden change in v_{in} profiles.

Formulas for the inward drift velocity derived from the particle balance prove that the contribution due to neutral injection must be taken into account. The inward drift velocity was shown to depend less than linearly on D which agrees with the results from modelling.

ACKNOWLEDGEMENT

The authors appreciate the support of the PPPL Transport Group and TFTR Physics Group by providing their BALDUR transport code.

References

/1/ Wagner, F., Becker, G., Behringer, K., Campbell, D., Eberhagen, A., et al., Phys. Rev. Lett. 49 (1982) 1408.

/2/ Wagner, F., Becker, G., Behringer, K., Campbell, D., Eberhagen, A., et al., Plasma Physics and Controlled Nuclear Fusion Research 1982 (Proc. 9th Int. Conf. Baltimore, 1982) Vol. 1, IAEA, Vienna (1983) 43.

/3/ Becker, G., ASDEX Team, Neutral Injection Team, Nuclear Fusion 22 (1982) 1589.

/4/ Becker, G., Campbell, D., Eberhagen, A., Gehre, O., Gernhardt, J., et al., Nuclear Fusion 23 (1983) 1293.

/5/ Becker, G., et al., Proc. 11th Europ. Conf. on Contr. Fusion and Plasma Physics, Aachen 1983, Vol. II, p. 299.

/6/ Post, D.E., Singer, C.E., McKenney, A.M., PPPL Transport Group, TFTR Physics Group, Report 33 (1981).

/7/ Becker, G., Singer, C.E., Proc. IAEA Techn. Comm. Meeting on Divertors and Impurity Control, Garching (1981) 63.

/8/ Becker, G., Singer, C.E., Report IPP III/75 (1981).

/9/ Chang, C.S., Hinton, F.L., Phys. Fluids 25 (1982) 1493.

/10/ Keilhacker, M., Lackner, K., Behringer, K., Murmann, H. and Niedermeyer, H., Physica Scripta Vol. T2/2 (1982) 443.

/11/ Ohkawa, T., Chu, M.S., Hinton, F.L., Liu, C.S. and Lee, Y.C., Phys. Rev. Lett 51 (1983) 2101.

Figure Captions

Fig. 1: Current I_p and line-averaged density $\bar{n}_e$ versus time. The transition to the H phase is marked by t^*.

Fig. 2: Computed $n_e(r)$ and $T_e(r)$ (solid curves) in the Ohmic phase compared with the density profile measured by HCN laser interferometry (dashed curve), quasi-stationary laser scattering (crosses) and Thomson scattering (circles), and with the T_e profile from ECE diagnostic (points) and Thomson scattering (circles).

Fig. 3: Profiles of χ_e, D and v_{in} during the Ohmic phase.

Fig. 4: As in Fig. 2, but in the H phase.

Fig. 5: Profiles of χ_e, D and v_{in} during the H phase. For comparison the v_{in} profile at 1.0 s is shown as a dashed curve.

Fig. 6: a) n_e profiles computed with the χ_e^L scaling of Eq. (2) (solid curve), and measured by Thomson scattering (triangles).
b) Computed $T_e(r)$ (solid curve) compared with T_e profile from Thomson scattering (triangles) and ECE diagnostic (circles).

Fig. 7: v_{in} profiles according to Eq. (3) with $(v_{in})_{max} = 300$ cm s^{-1} (dashed curves) compared with the prescribed $v_{in}(r)$ of Figs. 3 and 5 (solid curves).

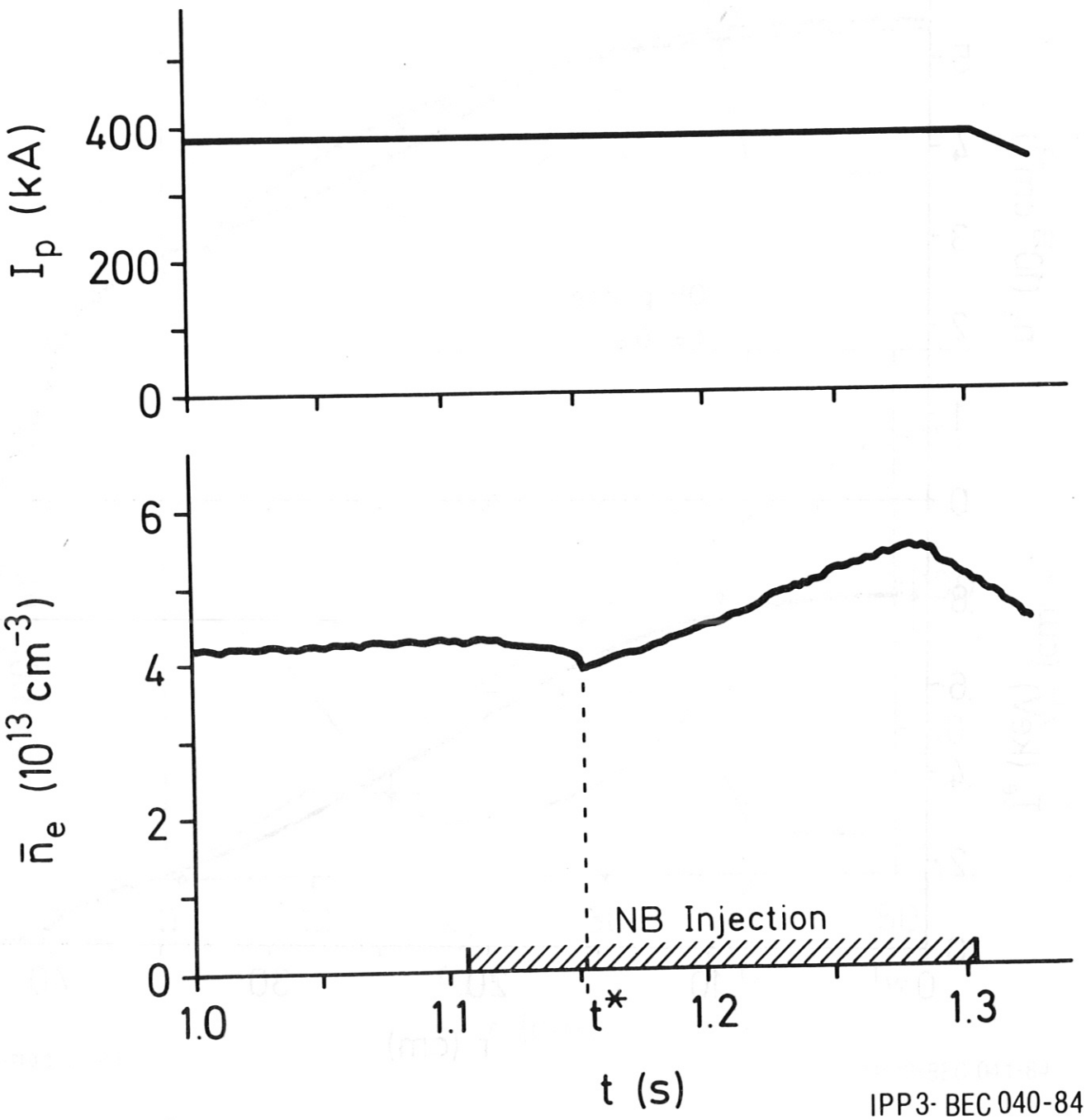
400
200
0
I_p (kA)
6
4
2
0
$\bar{n}_e$ (10^{13} cm^{-3})
NB Injection
1.0
1.1
t*
1.2
1.3
t (s)
IPP3- BEC 040-84

Fig. 1

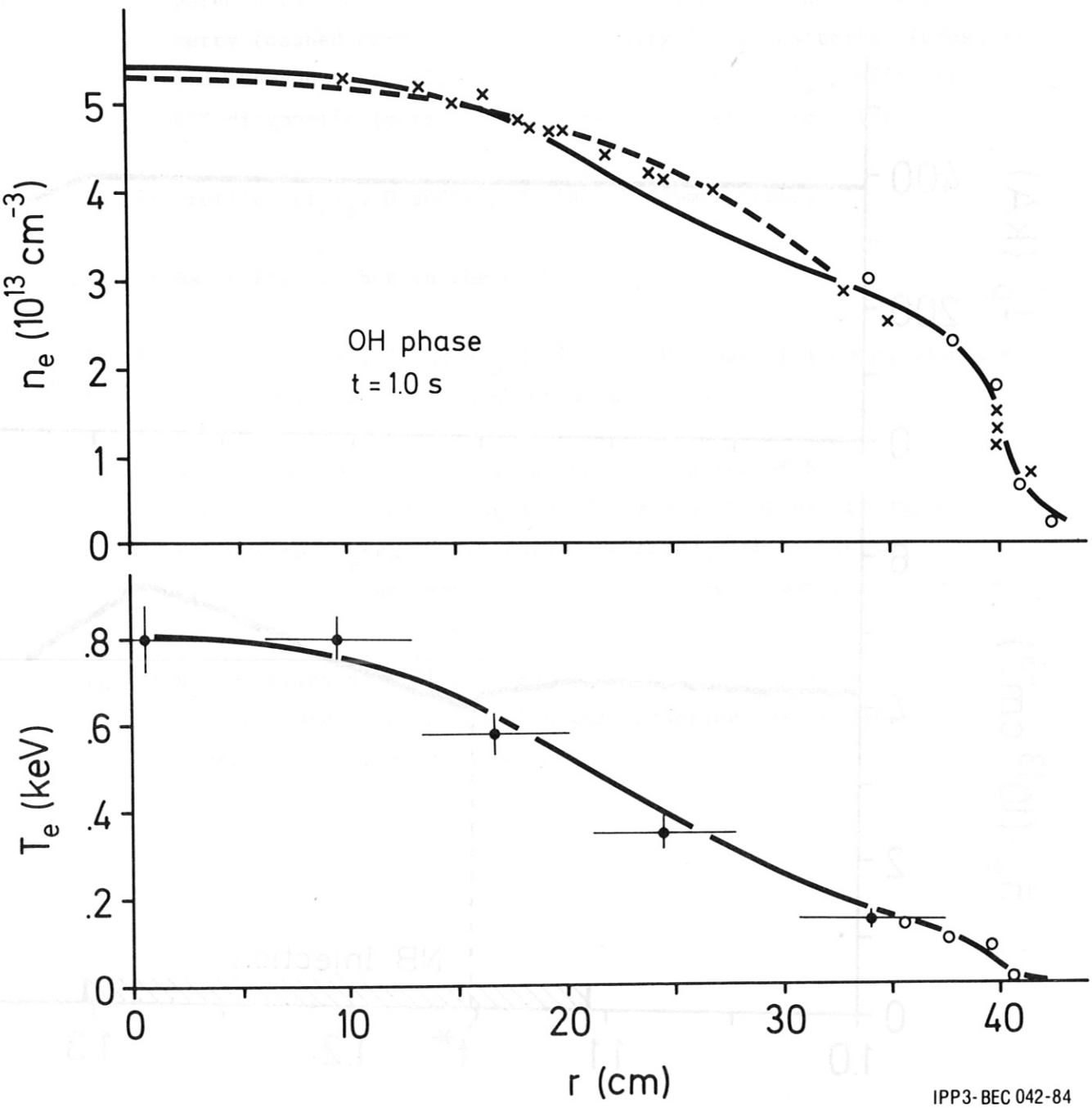

Fig. 2

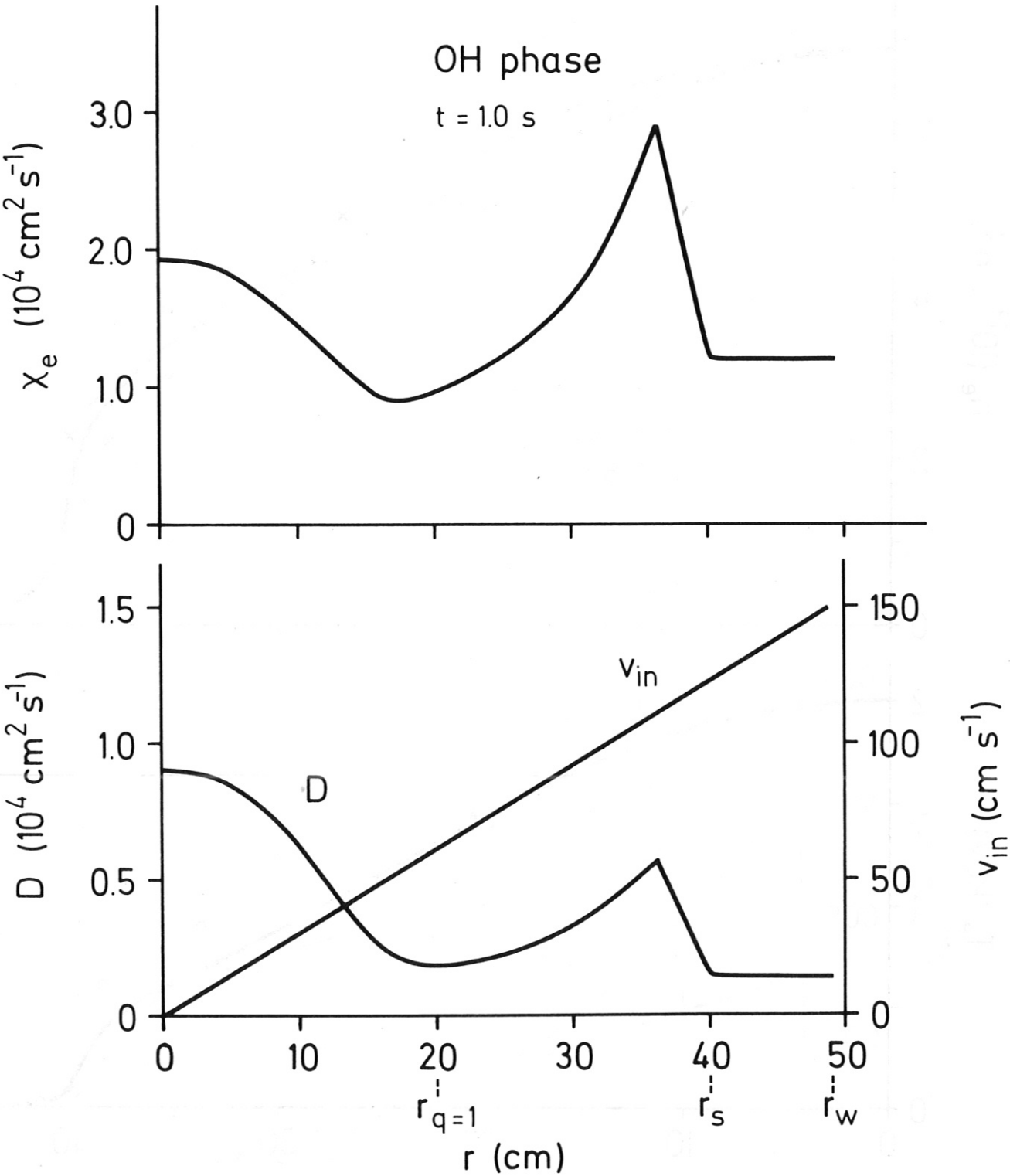
OH phase
t = 1.0 s
χ_e (10^4 cm^2 s^{-1})
3.0
2.0
1.0
0
D (10^4 cm^2 s^{-1})
1.5
1.0
0.5
0
D
v_{in}
150
100
50
0
v_{in} (cm s^{-1})
0
10
20
30
40
50
$r_{q=1}$
r_s
r_w
r (cm)
IPP3-BEC 041-84

Fig. 3

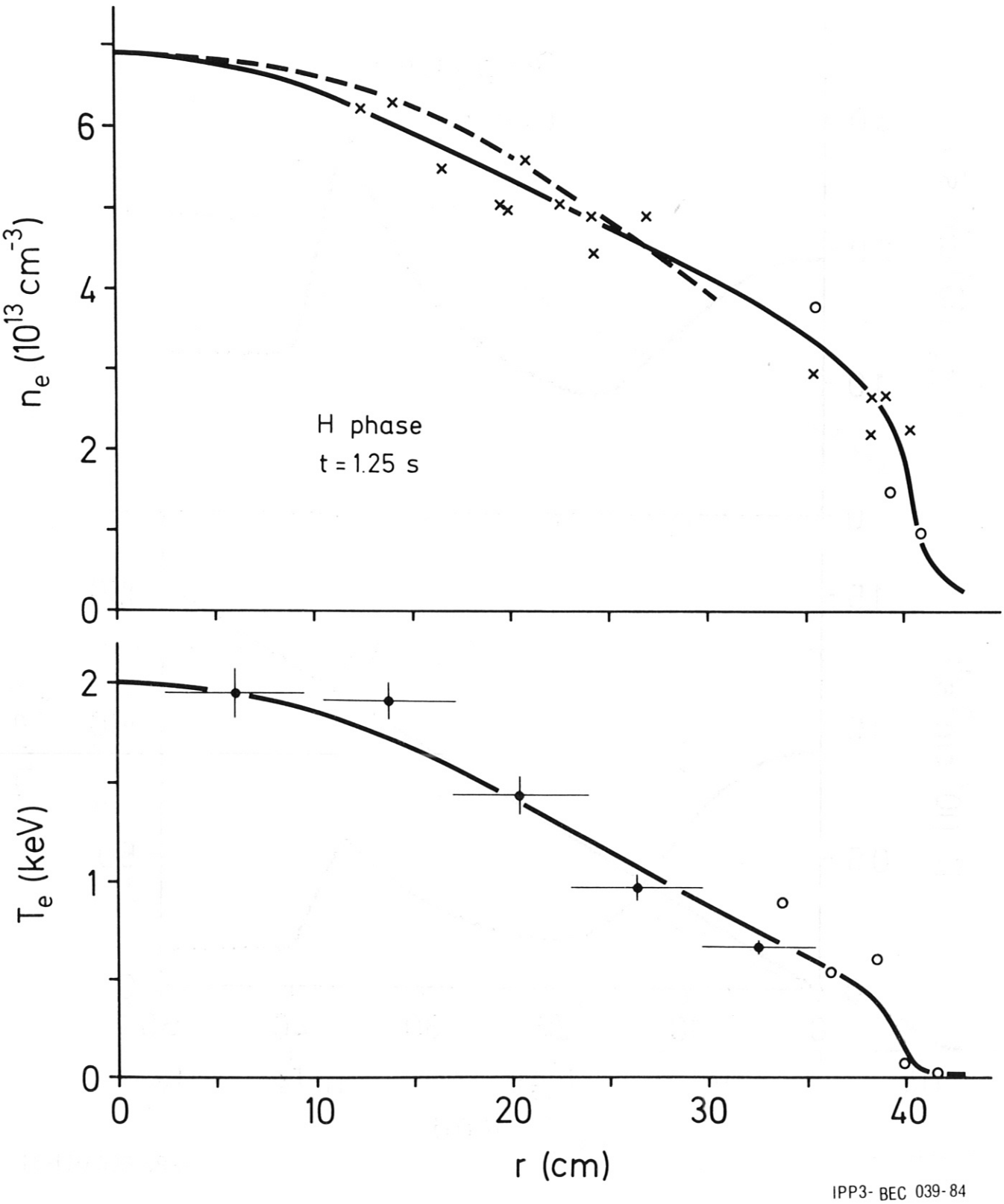
n_e (10^{13} cm^{-3})
6
4
2
0
H phase
t = 1.25 s
T_e (keV)
2
1
0
0
10
20
30
40
r (cm)
IPP3- BEC 039-84

Fig. 4

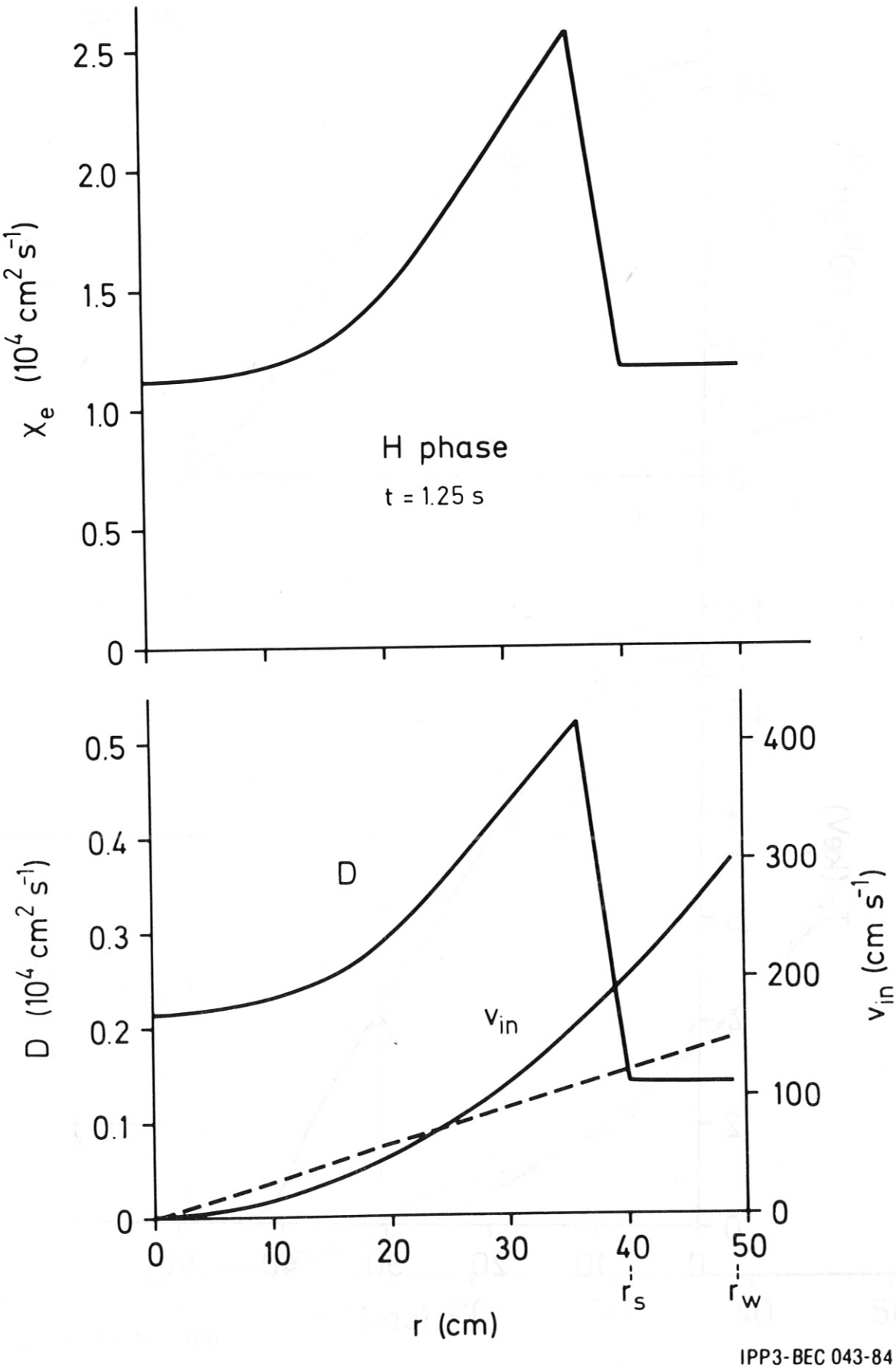
2.5
2.0
1.5
1.0
0.5
0
χ_e (10^4 cm^2 s^{-1})
H phase
t = 1.25 s
0.5
0.4
0.3
0.2
0.1
0
D (10^4 cm^2 s^{-1})
D
v_{in}
400
300
200
100
0
v_{in} (cm s^{-1})
0
10
20
30
40
50
r_s
r_w
r (cm)
IPP3-BEC 043-84

Fig. 5

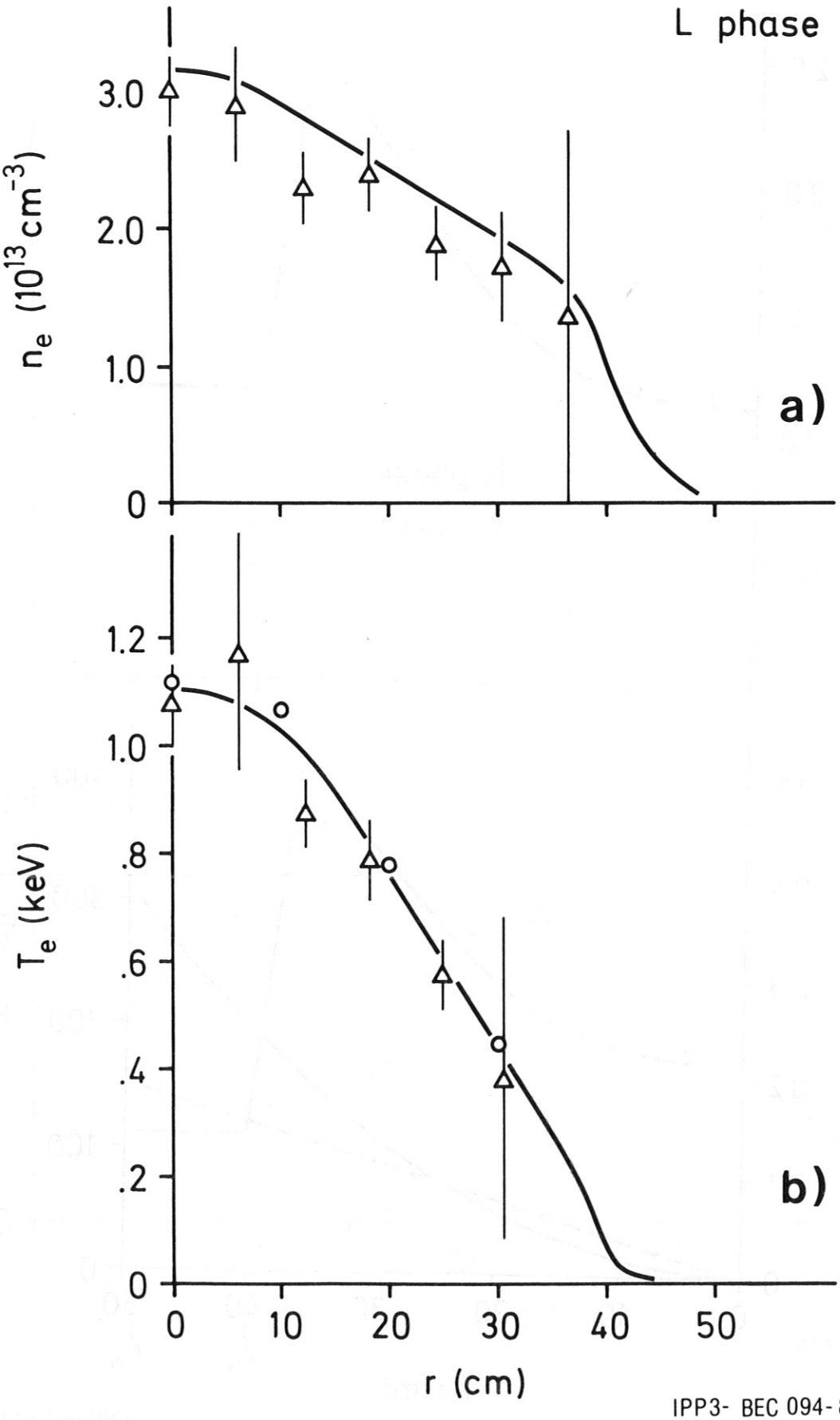
L phase
3.0
2.0
1.0
0
n_e (10^{13} cm^{-3})
a)
1.2
1.0
.8
.6
.4
.2
0
T_e (keV)
b)
0
10
20
30
40
50
r (cm)
IPP3- BEC 094-84

Fig. 6

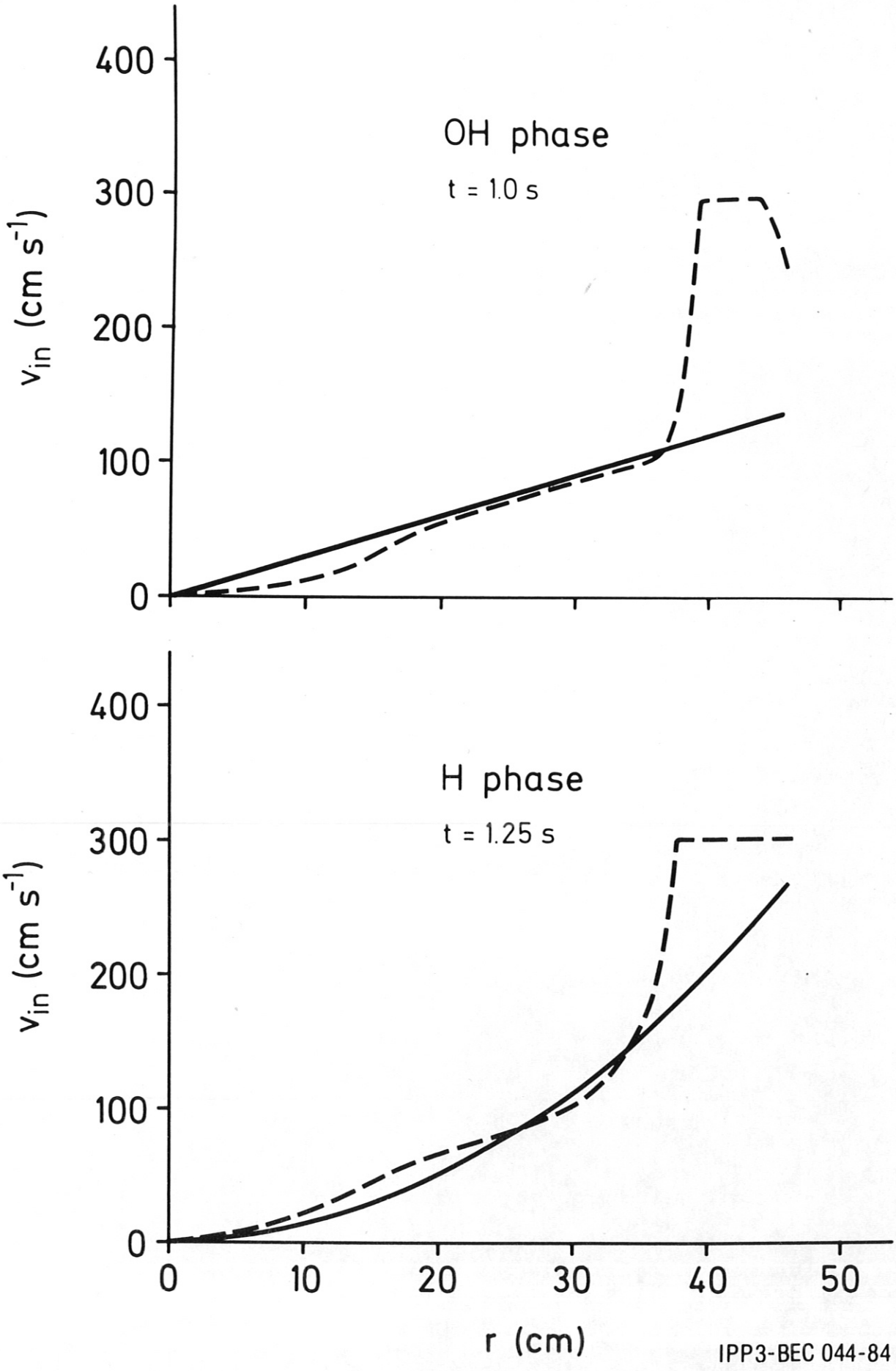
OH phase
t = 1.0 s
H phase
t = 1.25 s
v_{in} (cm s^{-1})
400
300
200
100
0
0
10
20
30
40
50
r (cm)
IPP3-BEC 044-84

Fig. 7